

Citation for published version:
Cargo, CJ, Hillis, AJ & Plummer, AR 2016, 'Strategies for active tuning of Wave Energy Converter hydraulic power take-off mechanisms', *Renewable Energy*, vol. 94, pp. 32-47. https://doi.org/10.1016/j.renene.2016.03.007

10.1016/j.renene.2016.03.007

Publication date: 2016

Document Version Peer reviewed version

Link to publication

Publisher Rights CC BY-NC-ND

Creative Commons Attribution Non-Commercial No Derivatives License

### **University of Bath**

### **Alternative formats**

If you require this document in an alternative format, please contact: openaccess@bath.ac.uk

**General rights** 

Copyright and moral rights for the publications made accessible in the public portal are retained by the authors and/or other copyright owners and it is a condition of accessing publications that users recognise and abide by the legal requirements associated with these rights.

If you believe that this document breaches copyright please contact us providing details, and we will remove access to the work immediately and investigate your claim.

Download date: 07, Mar. 2023

Strategies for active tuning of Wave Energy Converter hydraulic power take-off mechanisms

C.J. Cargo, A.J. Hillis\*, A.R. Plummer

Department of Mechanical Engineering, University of Bath, Bath BA27AY

Abstract

This paper presents a study of practically implementable active tuning methods

for a Wave Energy Converter (WEC) power take-off (PTO). It is distinguished

from other simulation studies by the level of detail and realism in the inputs and

the PTO model. Wave data recorded at the European Marine Energy Centre is

used to derive input data for a detailed component level model of a hydraulic PTO.

A methodology is presented for obtaining the optimum PTO damping co-efficient

for a given sea state, and an open loop active tuning method is used to adjust the

PTO parameters to achieve this optimum damping in service. The investigation

shows that tuning of a hydraulic PTO to an estimated wave frequency is a diffi-

cult task due to sea state estimation errors and the complex dynamics of a realistic

PTO. Preview knowledge of the future waves was shown to provide no meaningful

improvement in energy capture for the device under investigation. Significantly,

power gains observed in similar work using simplified linear PTO models or sim-

plified sea states are not seen here, demonstrating that over-simplification of the

PTO during the simulation phase of WEC development could lead to incorrect

design decisions and subsequent additional delay and cost.

Key words: wave energy, hydraulic PTO, power optimization, irregular waves

\*Corresponding author

Email address: a.j.hillis@bath.ac.uk (A.J. Hillis)

#### 1. Introduction

The optimization of wave energy converter (WEC) hydraulic power take-offs (PTO) in sea states of varying wave amplitude, direction, and frequency is a significant problem. Sub-optimal configuration can result in very inefficient energy conversion [1], so understanding the design trade-offs is key to the success of the technology. This work focuses on a generic point absorber type WEC. Previous work by the authors has considered the optimisation of this device for regular waves [2] and synthesised irregular waves [3] to gain an understanding of the fundamental issues. This paper considers real wave data from the European Marine Energy Centre (EMEC) based in Orkney, Scotland. It presents techniques to analyse the wave energy resource at a particular site by using statistics that are calculated 11 from the raw data. A method to calculate the wave excitation force from the raw 12 wave displacement is presented and this is then used as the input to a simulation 13 model. This provides a prediction of how the WEC will behave and the power 14 which can be generated in real wave conditions. 15 PTO tuning is investigated using the real data and compared to the results 16 found previously [2, 3]. Real time tuning methods are analysed to determine

PTO tuning is investigated using the real data and compared to the results found previously [2, 3]. Real time tuning methods are analysed to determine the best method to maximise power generation by updating the PTO damping. Active and passive methods are examined which tune the PTO to a wave frequency calculated from different horizons of wave data.

### 21 2. Background

Previous work has focused on developing control methods for point absorbers to maximize the energy absorbed. Falcao [4] used a simplified hydraulic PTO unit connected to a point absorber to develop an algorithm to optimize the converter. The algorithm was shown to be weakly dependent on wave period and independent of wave height when simulated in real sea conditions and to produce power levels similar to a fully linear PTO unit. This work was continued in Falcao [5] to include a strategy for phase control by latching to increase the absorbed power further. In Babarit et al. [6] three different latching control strategies are compared to show their effectiveness in different sea states with all three strategies giving a

considerably increased efficiency in irregular waves. In Yavuz et al. [7] work 31 focuses on assessing the performance of a tuneable point absorber by trying to fulfil 32 the condition of resonance by varying the PTO characteristics. Results showed a 33 maximum power capture of 50 per cent of the rated power in regular waves. This 34 work was continued in Yavuz et al. [8] with irregular waves to show that power capture can be maximized by continuously tuning the natural frequency of the 36 device to the incoming wave frequency. More recently, in Folley and Whittaker 37 [9], a new control method called active bipolar damping or declutching is proposed 38 which tries to shift the buoy's velocity so it is in phase with the wave force. When 39 compared theoretically to other methods, it shows a higher power capture than 40 optimum linear damping without the requirement of reactive energy storage. This 41 control method has been investigated in Babarit et al. [10] using a hydraulic PTO and compared to a control method which tries to mimic the continuous behaviour of a viscous damper. Results show greater power levels from the declutching control method with the added advantage of requiring a less complex system. Most of these 45 investigations use linearized models and do not consider real hydraulic circuits and components in their investigations. 47

#### $_{3}$ 3. Hydrodynamics of the WEC

A point absorber type device is used for this study and is the same as that used in [2] and [3]. A diagram of the heaving buoy is shown in Fig. 1, and it has a mass of 39 tonnes, a radius of 2m and a draft of 4m. A point mass acting at the centre of the buoy is assumed. The governing equation of motion for the buoy in heave is

$$m\ddot{x} = f_h(t) + \Phi(t) \tag{1}$$

where m is the mass of the buoy,  $\ddot{x}$  is the buoy's acceleration,  $f_h(t)$  is the total wave force and  $\Phi(t)$  is the mechanical force created by the PTO and moorings. Assuming linear wave theory, the wave force can be approximated as

$$f_h(t) = f_e(t) + f_r(t) + f_{hs}(t)$$
 (2)

where  $f_e(t)$  is the excitation force produced by an incident wave on an otherwise fixed body,  $f_r(t)$  is the radiation force and  $f_{hs}(t)$  is the hydrostatic buoyancy force. For a regular wave of frquency  $\omega$  the excitation force is given by

$$f_e(t) = Re(F_e e^{j\omega t}) \tag{3}$$

where  $F_e$  is the complex excitation force amplitude. Following the approach described in [3] and using the assumptions of [11] and Hulme [12], for a hemispherical body that is small in comparison to the incident wavelength,  $F_e$  may be approximated by

$$F_e \approx \frac{H\rho}{\omega} \sqrt{\frac{\pi}{3} g^3 r^3 \epsilon e^{-2kl}} \tag{4}$$

where H is the free surface elevation,  $\rho$  is the water density, g is the acceleration due to gravity, r and l are the radius and half-height of the buoy,  $\epsilon$  is Havelock's dimensionless damping coefficient computed by Hulme [12] and k is the wave number  $(k = \frac{\omega^2}{g})$  given by the deep water dispersion equation.

The radiation force  $f_r(t)$  can be decomposed into components in phase with the buoy's acceleration and velocity [11] [13] so that

$$f_r(t) = -A(\omega)\ddot{x} - B(\omega)\dot{x} \tag{5}$$

where  $A(\omega)$  is the added mass coefficient and  $B(\omega)$  is the radiation damping coefficient, which may be approximated in this case to [11] [12]

$$B(\omega) \approx \omega \rho \left(\frac{2\pi}{3}\right) r^3 \epsilon e^{-2kl}$$
 (6)

For small heave displacements, the hydrostatic force  $f_{hs}(t)$  can be linearised so that

$$f_{hs}(t) = -\rho g \pi r^2 x \tag{7}$$

#### 74 4. Hydraulic PTO mechanism

The aim of the PTO is to convert the irregular wave input into a smooth electrical power output by decoupling the power capture and power generation

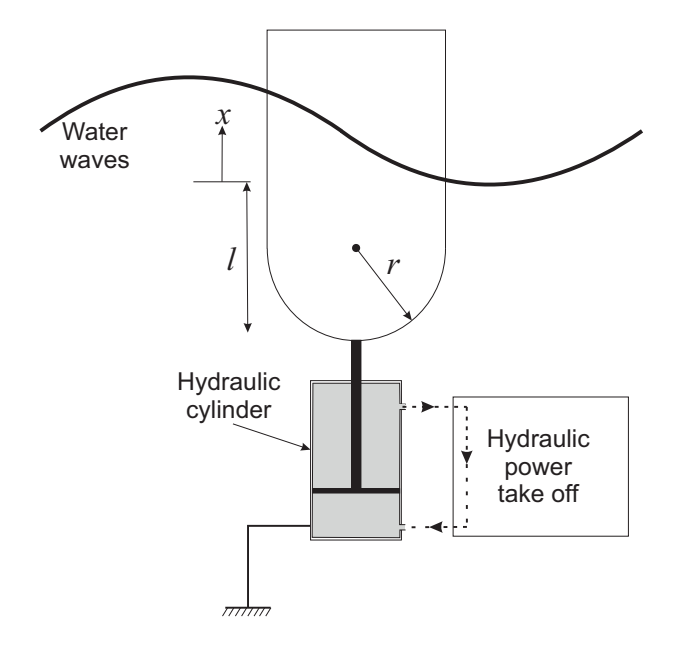


Figure 1: Schematic diagram of the WEC

processes. Hydraulic PTOs are generally used in WECs due to their advantages for dealing with low frequency, high force wave inputs and their high power density and robustness.

The hydraulic PTO used in this simulation model is shown in Figure 2. The 80 simplified circuit excludes components such as filters and coolers which would 81 be required in the real hydraulic system. The heave motion of the buoy drives a double-acting equal area hydraulic piston within a fixed cylinder to pump hydraulic 83 oil through rectification circuit to provide unidirection flow through a hydraulic 84 motor. The pressure difference between the high and low pressure accumulators 85 drives a variable displacement hydraulic motor, which drives an electrical gener-86 ator. The accumulators are intended to smooth the pressure differential across 87 the hydraulic motor and therefore achieve synchronous power generation. The 88 thermodynamic transformations in the accumulators are assumed to be isentropic, which is a reasonable assumption considering the cycle time of the device. The 90 generator is modelled as a simple rotational damper with variable damping coef-91 ficient allowing its resistive torque to be altered. In a real circuit, there will be external leakage from the motor to tank. Therefore, to replenish the circuit and 93 avoid cavitation in the cylinder, an additional accumulator is used to maintain a 94 minimum system pressure of 10 bar. Pressure relief valves are used to limit the

peak system pressure to 350 bar and protect hydraulic components.

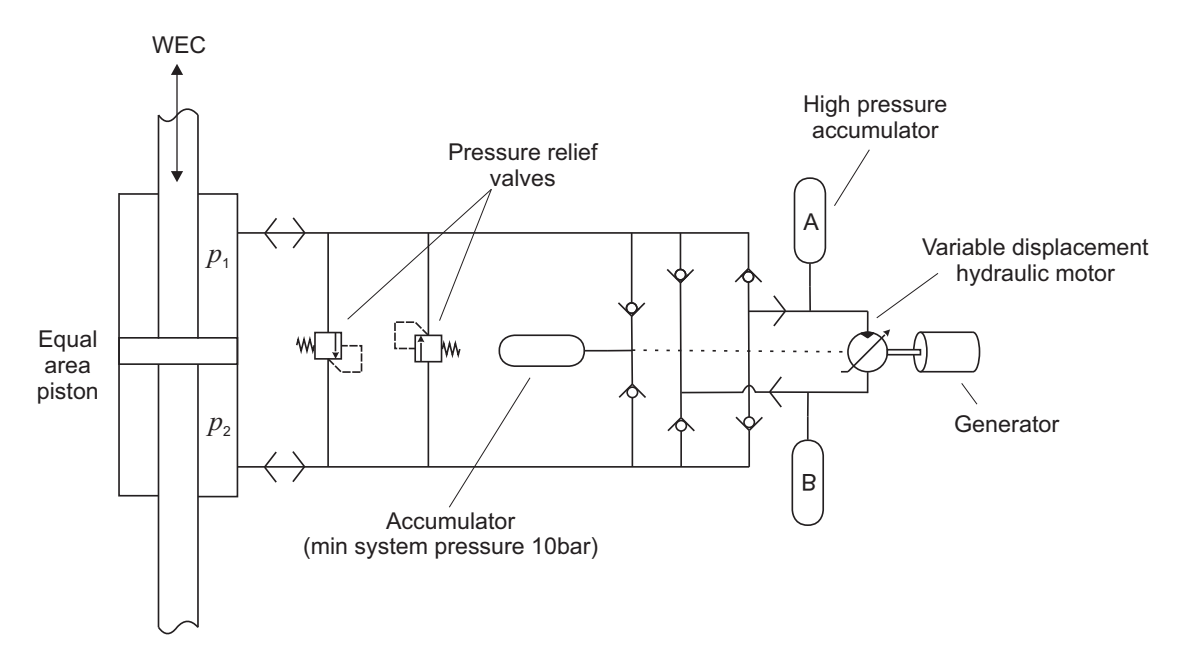


Figure 2: Hydraulic PTO circuit diagram

In reality there will be losses throughout the hydraulic circuit including friction in the piston and pipework, leakage in the motor and torque losses due to friction in the motor and generator. These losses will be system specific and are approximated here based on experience.

The PTO force is given by

$$\Phi = (p_1 - p_2)A_p - f_{fr} \tag{8}$$

where  $p_1$  and  $p_2$  are the pressures in the piston chambers,  $A_p$  is the piston area and  $f_{fr}$  is the cylinder friction force, given by

$$f_{fr} = f_c sign(\dot{x}) + f_v \dot{x} \tag{9}$$

where  $f_c$  and and  $f_v$  are the Coulomb and viscous friction coefficients, respectively.

The details for calculating cylinder pressures are provided in [3].

The mechanical power captured by the PTO is given by

$$P_{cap} = \Phi \dot{x} \tag{10}$$

The power generated by the PTO is not equal to the captured power  $P_{cap}$  due to system losses in the hydraulic circuit and electrical generator. The generated power may be caluclated from

$$P_{gen} = T_m \omega_m \tag{11}$$

where  $T_m$  and  $\omega_m$  are the motor torque and angular velocity, respectively. The motor torque is calculated from [14]

$$T_m = x_m D_m (p_A - p_B) - C_f D_m (p_A - p_B) - C_v D_m \mu \omega_m$$
 (12)

where  $x_m$  is the fraction of maximum displacement  $D_m$  of the hydraulic motor displacement,  $\mu$  is the dynamic viscosity of the oil and  $p_A$  and  $p_B$  are the accumulator pressures. Again, the details for calculating accumulator pressures are provided in [3].  $C_v$  and  $C_f$  are dimensionless viscous friction and Coulomb friction co-efficients representing motor losses according to the Wilson model [14]. Slip losses are also included, and are calculated as[14]

$$q_m - \frac{C_s D_m (p_A - p_B)}{\mu} = x_m D_m \omega_m \tag{13}$$

where  $q_m$  is the flowrate to the motor and  $C_s$  is the dimensionless slip coefficient. The motor angular velocity can be calculated from rotational acceleration, which is given by

$$\dot{\omega}_m = \frac{T_m - T_g}{J} \tag{14}$$

where  $T_g$  and J are the torque and inertia of the generator.

Assuming no losses, the generator torque is given by

$$T_g = C_g \omega_m \tag{15}$$

where  $C_g$  is the damping coefficient of the generator.

Table 1 shows the component parameters in the PTO. These values are not based on any specific design but are a representation of suitable sizing for the buoy size. In this idealised case the effect of the boost pump is negligible and the

electrical generator is assumed to be 100% efficient so the electrical power generated can be equated to the mechanical power generated by the PTO. The high pressure accumulator ('A') has a relatively low pre-charge pressure to ensure that it charges even in calm wave conditions.

Maximum system pressure	$350\mathrm{bar}$
Equal area piston	
Area	$0.007\mathrm{m}^2$
Stroke Limit	$\pm 2.5\mathrm{m}$
HP Gas accumulator 'A'	
Pre-charge Pressure	$30\mathrm{bar}$
Volume	$200\mathrm{L}$
$\gamma$	1.4
LP Gas accumulator 'B'	
Pre-charge Pressure	$10\mathrm{bar}$
Volume	$200\mathrm{L}$
$\gamma$	1.4
Variable Displacement Motor	
Capacity	$180\mathrm{cc/rev}$
Generator	,
Damping coefficient	$2.5  \mathrm{Nm/(rad/s)}$
Inertia	$2  \mathrm{kgm}^2$
Oil Properties	O
Viscosity	$50\mathrm{cSt}$
Density	$850\mathrm{kg/m^3}$

Table 1: PTO component values

Table 2 shows the parameters of all the other components required to calculate the losses.

Cylinder	
Coulomb friction $(f_c)$	$3500\mathrm{N}$
Viscous friction coefficient $(f_v)$	100  N/(m/s)
Variable Displacement Motor	
$C_f$	0.014
Check Valve	
Valve constant $(K_v)$	$8.5 \times 10^{-6}$
Cracking Pressure	$0.3\mathrm{bar}$
Pipework	
Diameter $(d)$	$50\mathrm{mm}$
Total Length $(l)$	$10\mathrm{m}$

Table 2: PTO unit component loss parameters

#### 5. Wave Data Analysis

Real ocean waves are random but there are key parameters which can be 134 calculated from recorded wave elevation data to analyse and compare different 135 sea states. These parameters are calculated from the frequency moments of the 136 variance spectrum  $(m_a)$  [15]. The frequency spectrum  $(S_n)$  is given by the Fast 137 Fourier Transform (FFT) of the wave elevation. Figure 3 shows the spectrum as 138 a result of taking the FFT of a 30 minute duration data packet sampled at 139 1.28Hz. The raw FFT produces a noisy spectrum which could produce erroneous 140 results when used to calculate key parameters of the underlying sea state. A 141 smoothed spectrum may be obtained by passing the raw amplitude spectrum 142 through a polynomial filter. In this case a Savitzky-Golay filter was used [16], 143 though this is arbitrary. A third order polynomial filter was used with a frame 144 size of 81. In subsequent analyses, both raw and smoothed spectra are used for 145 PTO tuning and the results are compared. 146

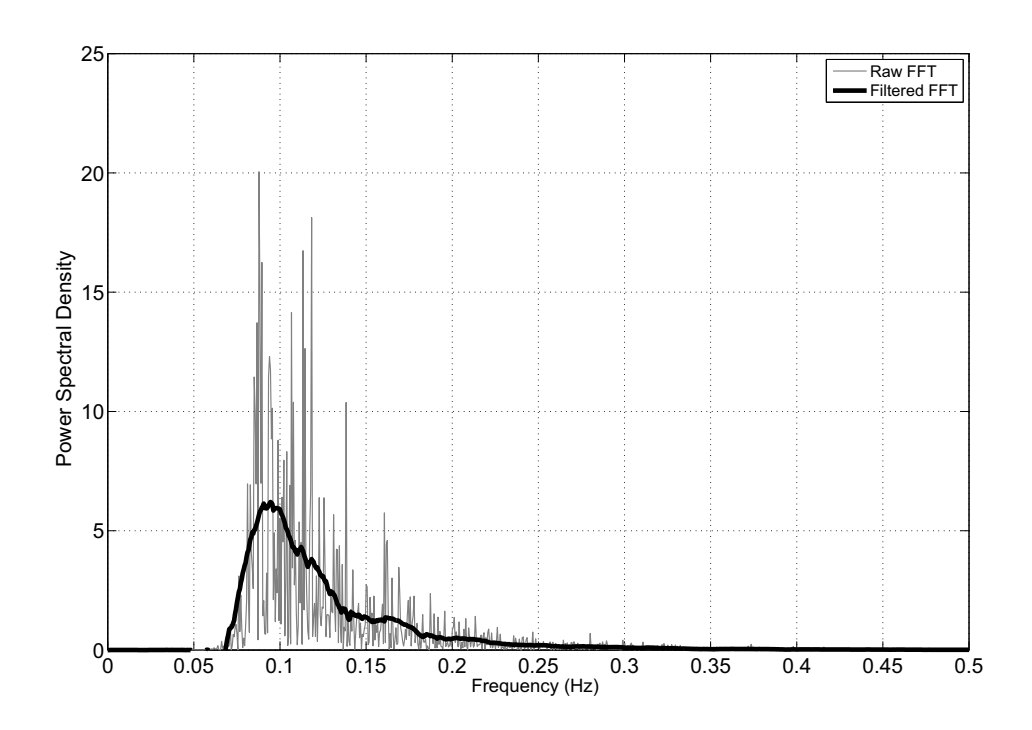


Figure 3: Example frequency spectrum of measured wave data

The moments of the variance spectrum  $(m_a)$  for a=-1,0,1,2, are calculated from

148 [15]:

$$m_a = \sum_{i=1}^{N} S_{n_i} \omega_i^a \Delta \omega = \int_0^{\omega_N} S_n \omega^a d\omega$$
 (16)

where N is chosen so as to include the frequency range ( $\omega_i$  to  $\omega_N$ ) containing significant power (e.g. 0-0.25Hz in Figure 3.) The significant wave height ( $H_s$ ), peak period ( $T_p$ ), energy period ( $T_e$ ) and wave power flux ( $P_{flux}$ ) are key parameters[15]. The significant wave height is the average of the wave heights of the third largest waves and the peak period is the wave period corresponding to the most energetic waves in the spectrum and is given by

$$H_s = 4\sqrt{m_0} \tag{17}$$

The peak period  $T_p$  is given by

$$T_p = \frac{1}{f_p} \tag{18}$$

where  $f_p$  is the frequency in Hz corresponding to maximum  $S_n$ .

The energy period  $(T_e)$  is given by

$$T_e = \frac{m_{-1}}{m_0} \tag{19}$$

The total wave power flux  $(P_{flux})$  of the spectrum is the scalar sum over the frequency range, and is found from

$$P_{flux} = \frac{1}{2a} \sum_{i=1}^{N} P_{wave_i} \tag{20}$$

Artificial irregular wave elevation and excitation force profiles can be created using the random-phase method [5] though this results in periodic signals which are not realistic. Alternatively, they can be generated by shaped filtering of white noise [17, 18] which is more realistic. Real waves are non repeating and their frequency spectrum may have more than one significant peak. This work uses real wave data collected from test sites to determine if the trends and methods which have been found previously [2] are applicable to real waves.

EMEC has a number of data collection buoys in different locations around their

site in Orkney. Data for the months of April and October 2011 were obtained for 169 one of the locations (Billia Croo Buoy E). The data is for the wave heave 170 displacement and it is split into 30 minute packets with a sampling frequency of 171  $1.28\,\mathrm{Hz}.$ 172 The wave parameters defined in equations 17 to 20 were calculated for each individual data packet and the results for both months are compared in Figures 4 174 to 7. They reveal that the average power available in April was lower than 175 October. October had more occurrences of the lowest level of wave power 176 (<30 kW/m) but there were also more large wave powers (>100 kW/m), which 177 indicates more variable weather (Figure 7). The average values of terms relating 178 to wave period are lower for October but the variance is lower in April. In 179 particular, there are more short period waves in October (Figure 5). This may 180 indicate a changing of the dominant wave frequency through the year in this 181 location. 182

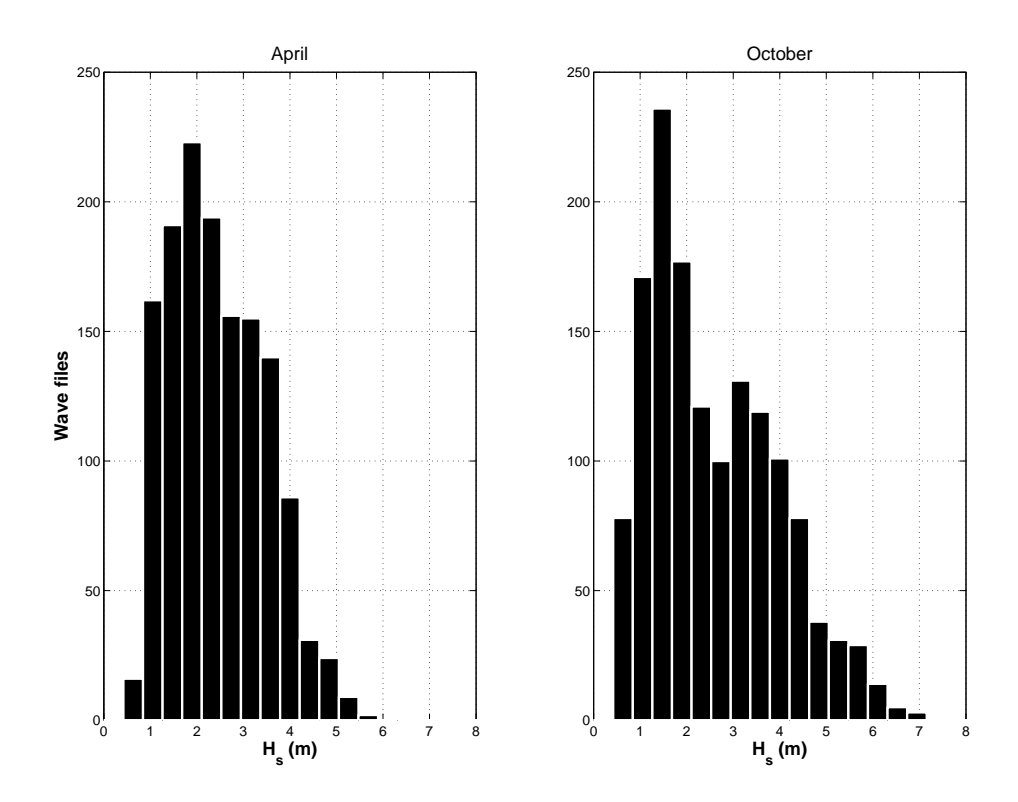


Figure 4: Frequency histogram showing the significant wave height in April and October

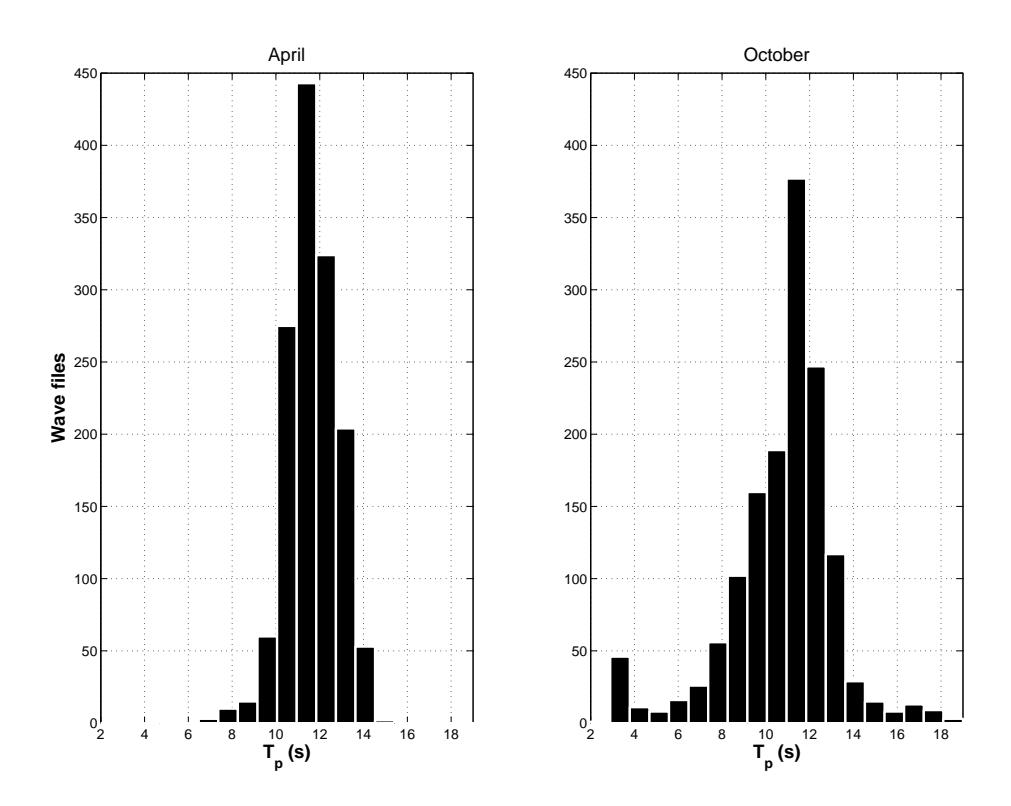


Figure 5: Frequency histogram showing the peak period in April and October (from filtered spectrum)

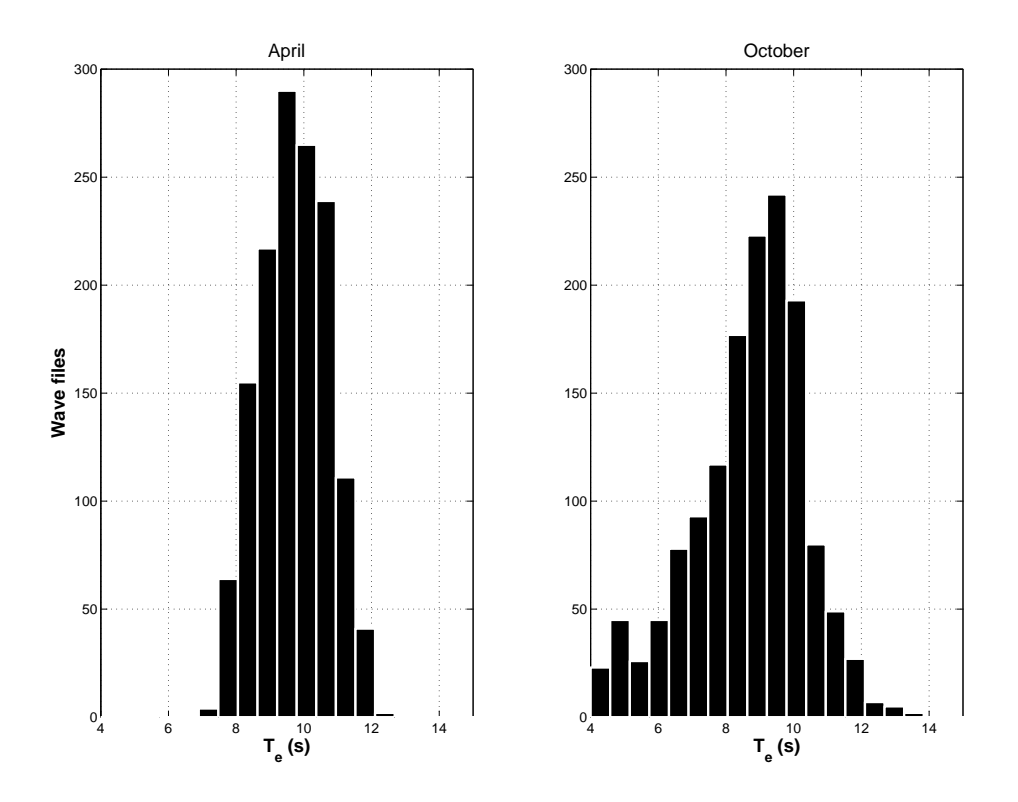


Figure 6: Frequency histogram showing the energy period in April and October

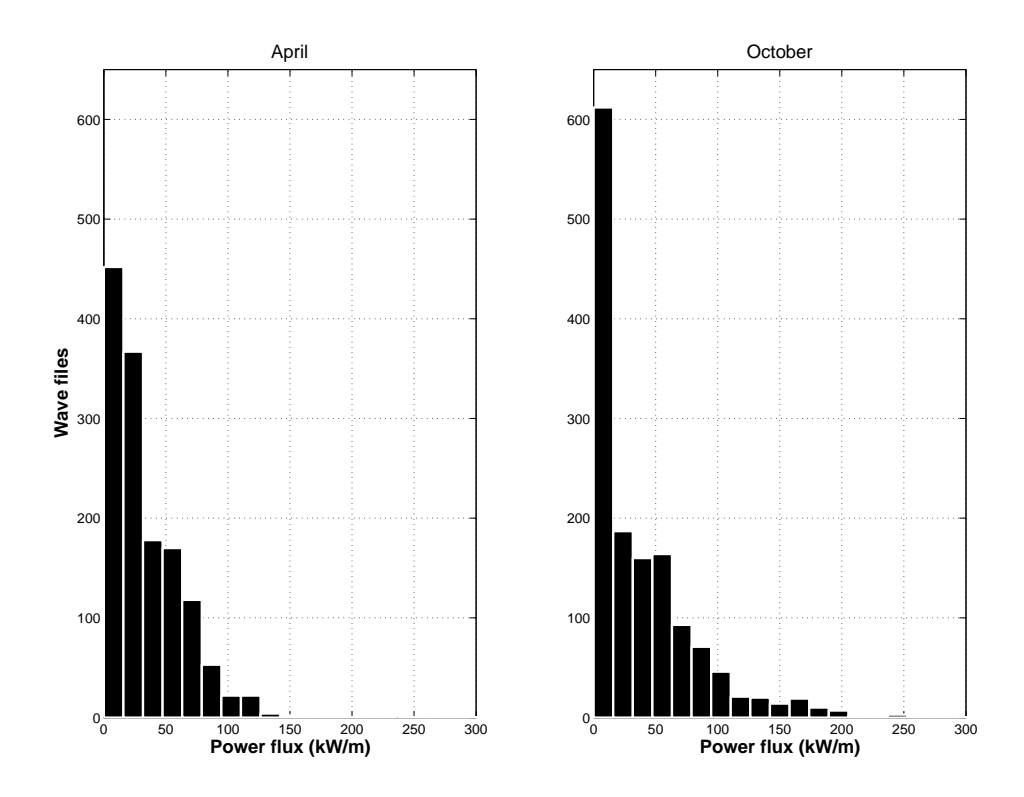


Figure 7: Frequency histogram showing the wave power flux in April and October

# 6. Generating a Wave Excitation Force Signal from wave elevation data

184

The simulation model uses wave excitation force as the input to the 185 hydrodynamic model so it is necessary to create a wave excitation force signal 186 from the wave elevation data. The FFT of the wave displacement gives the 187 discrete frequency components  $(\omega_i)$  and their corresponding amplitude  $(X_{w_i})$  and 188 phase  $(\phi_i)$ . Assuming a finite number of wave components, the wave excitation 189 force coefficient  $\Gamma(\omega_i)$  of each wave component can be calculated as follows. 190 Equations 4 and 6 can be combined to obtain an expression for the wave 191 excitation force amplitude  $F_e$  as a function of the radiation damping coefficient 192  $B(\omega)$ : 193

$$F_e \approx H \sqrt{\frac{B(\omega)g^3\rho}{2\omega^3}} \tag{21}$$

According to Falnes [11], Fe can be expressed in terms of the wave excitation force coefficient  $\Gamma(\omega)$  as:

$$F_e = \Gamma(\omega) \frac{H}{2} \tag{22}$$

196 Comparing equation 21 with equation 22, it can be seen that

$$\Gamma(\omega_i) = \frac{2}{H} F_e \approx \sqrt{\left(\frac{2g^3 \rho B(\omega_i)}{\omega_i^3}\right)}$$
 (23)

The excitation force can then be calculated from

$$f_e(t) = \sum_{i=1}^{n} \Gamma(\omega_i) X_w(\omega_i) \cos(\omega_i t + \varphi_i)$$
 (24)

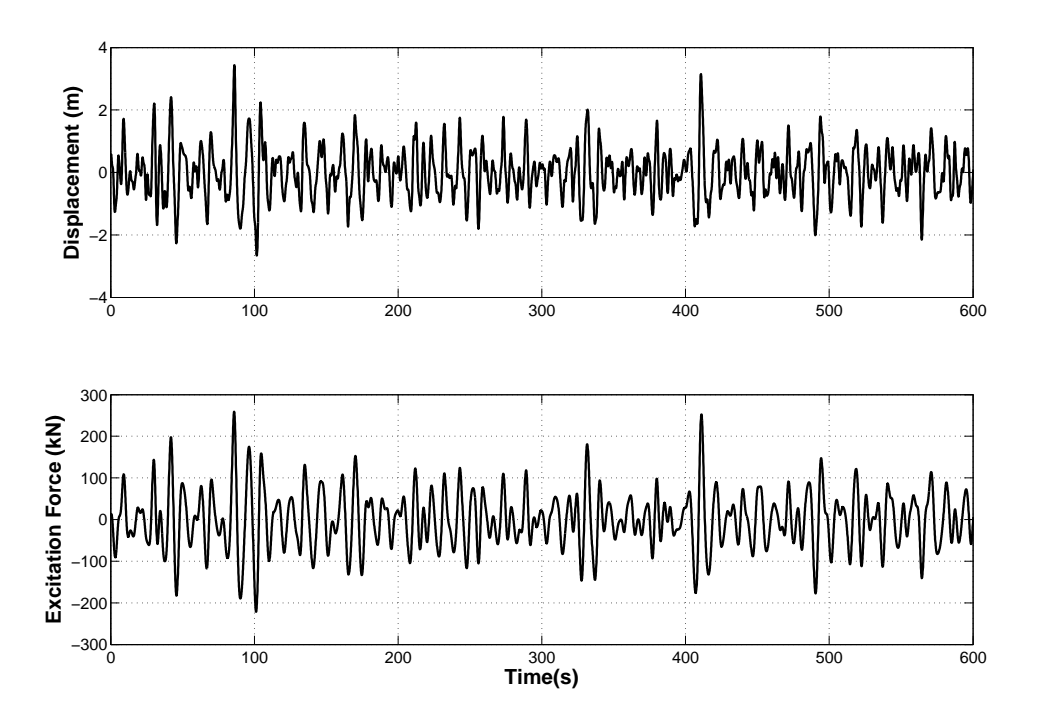


Figure 8: Wave displacement and excitation force for an example EMEC file

- Figure 8 shows a 600 s section of an example EMEC file with the wave
- displacement and the calculated wave excitation force. In the time domain,
- 200 Figure 9 shows that the WEC behaves in a similar manner to that in irregular
- waves produced by the random phase method [2], with induced body stall and
- 202 Coulomb type PTO force evident.
- 203 Since the wave profile is non-repeating the energy stored in the accumulators will
- 204 not achieve a pseudo-steady state over a fixed time period as seen with a

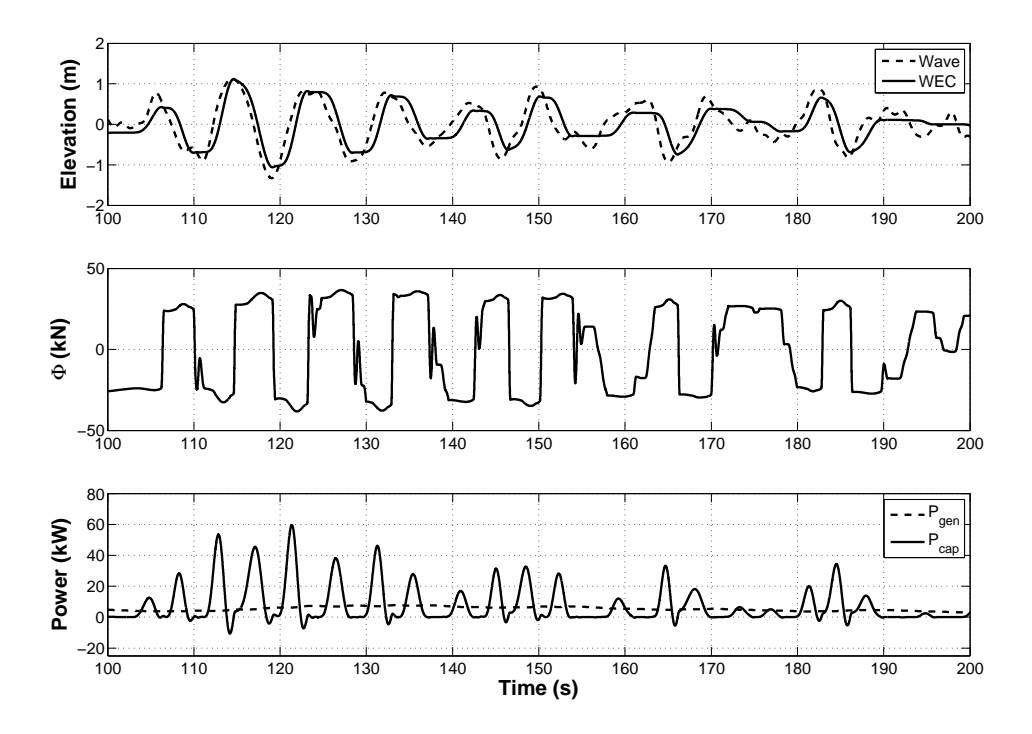


Figure 9: WEC and PTO behaviour in the example EMEC file

repeating wave force input [3]. Therefore, to negate the effect of the added energy stored in the accumulators giving an inaccurate result for the generated power  $(P_{gen})$  and PTO efficiency  $(\eta_{pto})$  the model is analysed over the largest possible time period.

#### 7. PTO Tuning in Real Seas

Previous work [3] demonstrated a relationship between the peak wave period  $(T_p)$ and the optimum PTO damping  $(\alpha_{opt})$  for waves created using the Pierson-Moskowitz spectrum and the random phase method:

$$\alpha_{opt}(T_p) = C_g \left(\frac{x_m D_m}{A_p}\right)^2 \tag{25}$$

where  $A_p$  represents the piston area,  $C_g$  is the generator damping coefficient,  $D_m$  is the hydraulic motor capacity and  $x_m$  is the fraction of maximum motor displacement. Here, the piston area is fixed and the PTO damping is optimised for a given  $T_p$  by varying the motor capacity and generator load.

It is important to determine if this, or any other relationship, exists for real wave

data. Therefore, a number of wave packets were chosen in both months with  $H_s \approx 2.5 \,\mathrm{m}$  and  $T_p$  ranging from 8-14s approximately. For each of the wave packets an optimisation algorithm was used to maximise  $P_{gen}$  and give  $\alpha_{opt}$  to determine any trends between it and the wave parameters.

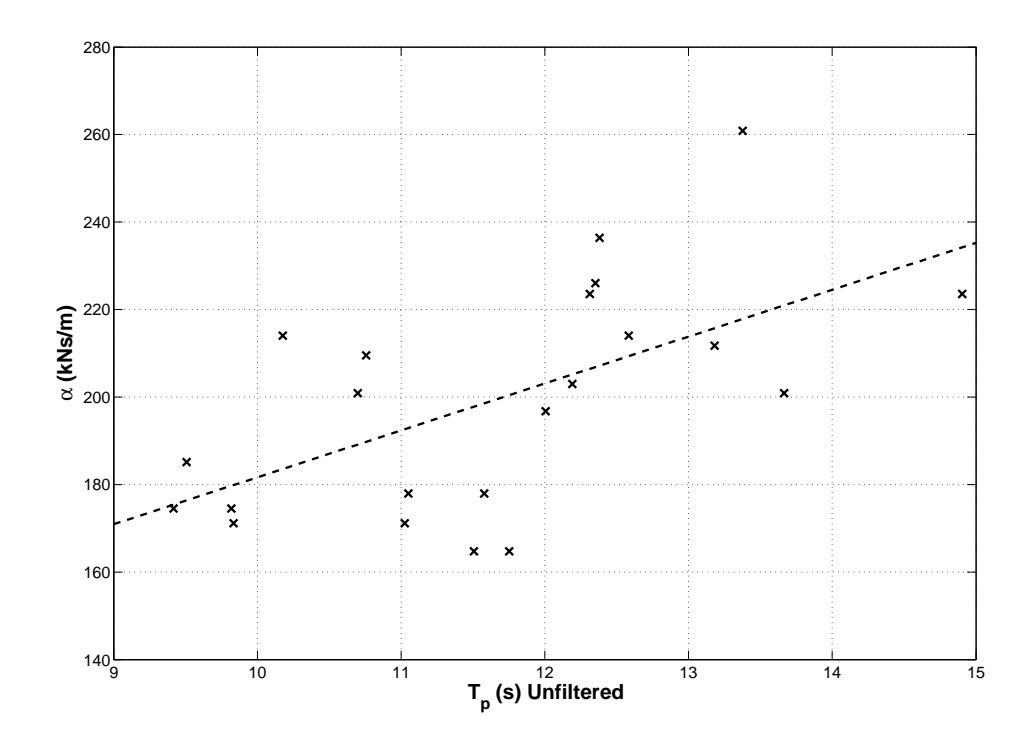


Figure 10: Optimum PTO damping vs peak wave period with filtered spectrum

Wave Parameter	Hydraulic PTO
$T_p$ (Filtered)	74.9
$T_p$ (Unfiltered)	95.3
$T_e$	56.1

Table 3: Norm of the residuals for the fit between the optimum PTO damping and the different wave parameters

Figures 10, 11 and 12 show that the correlation between  $T_p$  and  $\alpha_{opt}$  is better when  $T_p$  is calculated from the filtered spectrum. However, Table 3 shows that the norm of the residuals, an indicator of the goodness of the correlation, is lowest for the fit between the energy period  $(T_e)$  and  $\alpha_{opt}$ .

When comparing all the trend lines, it is clear from Figure 13 that the filtered  $T_p$  and unfiltered  $T_p$  trends are very similar. It also shows that the trend for  $T_e$  and  $T_p$  using a Pierson-Moskowitz spectrum are similar. In terms of power, Figure 14

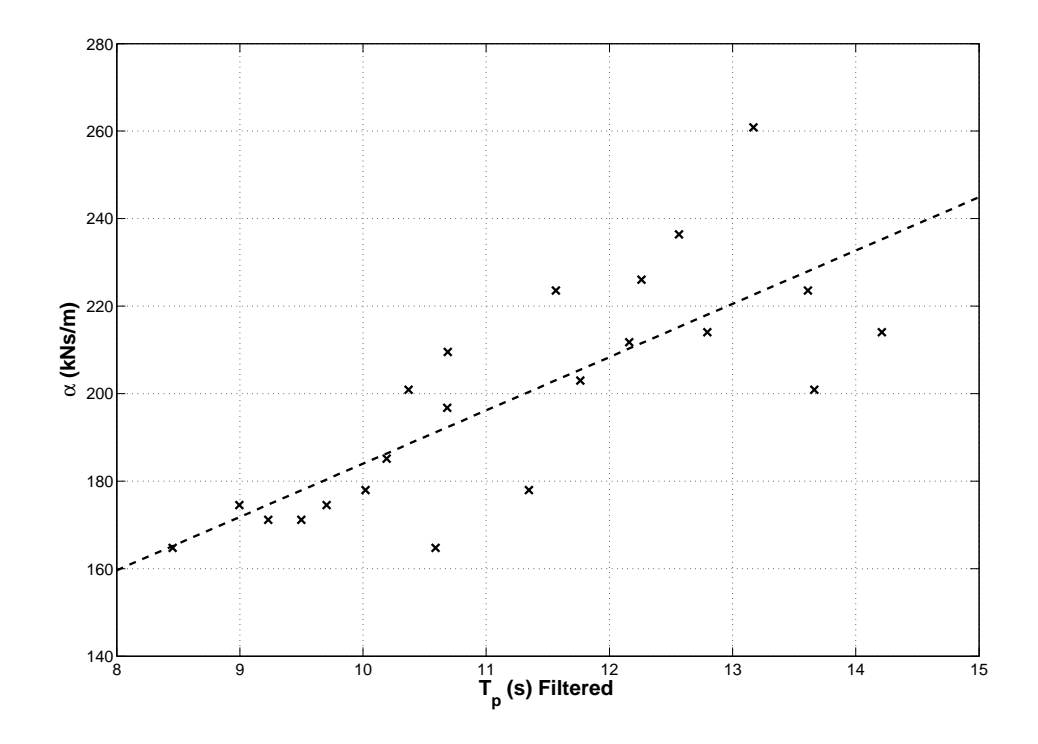


Figure 11: Optimum PTO damping vs peak wave period with unfiltered spectrum

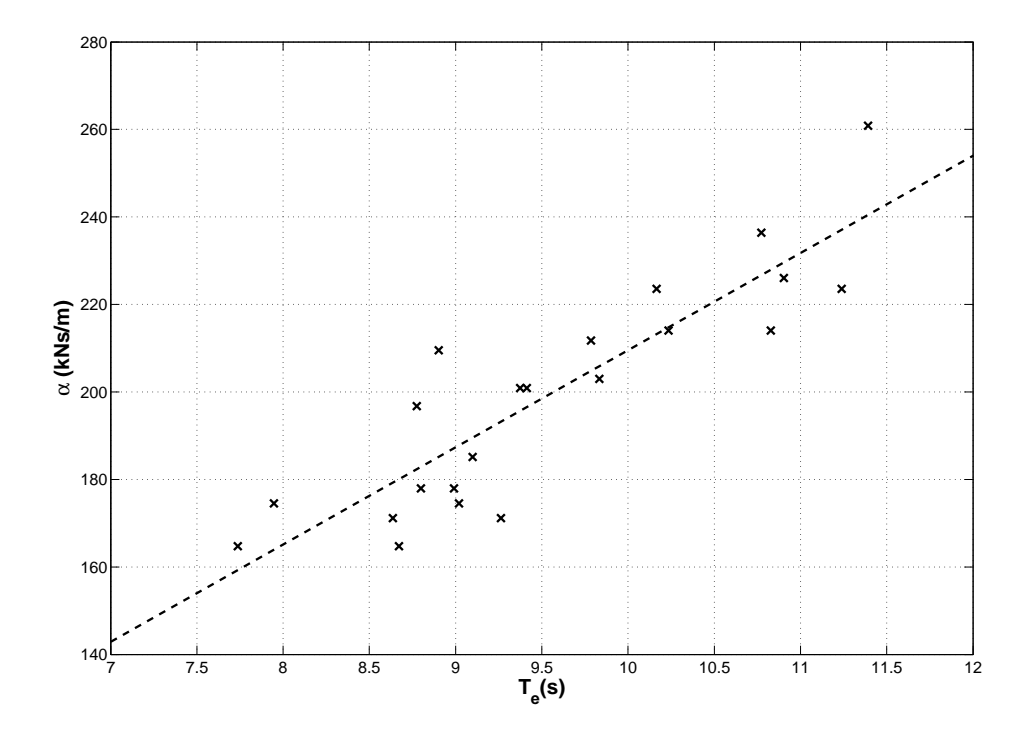


Figure 12: Optimum PTO damping vs energy period

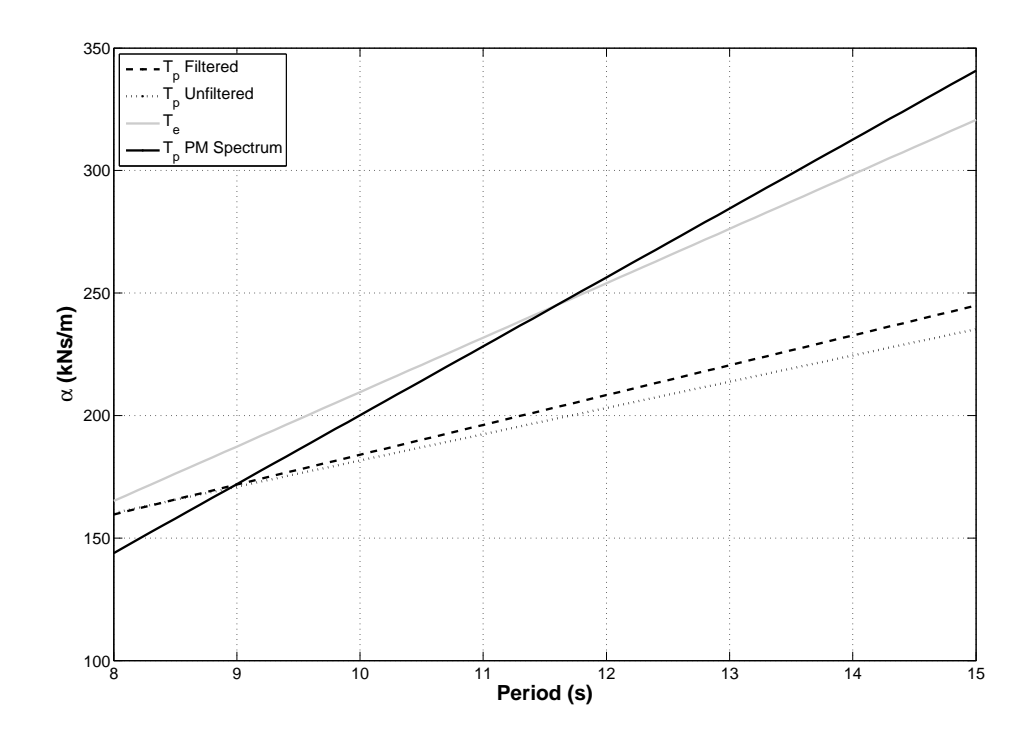


Figure 13: Comparison of the optimum PTO damping trends for the hydraulic PTO for different wave parameters  ${\cal P}$ 

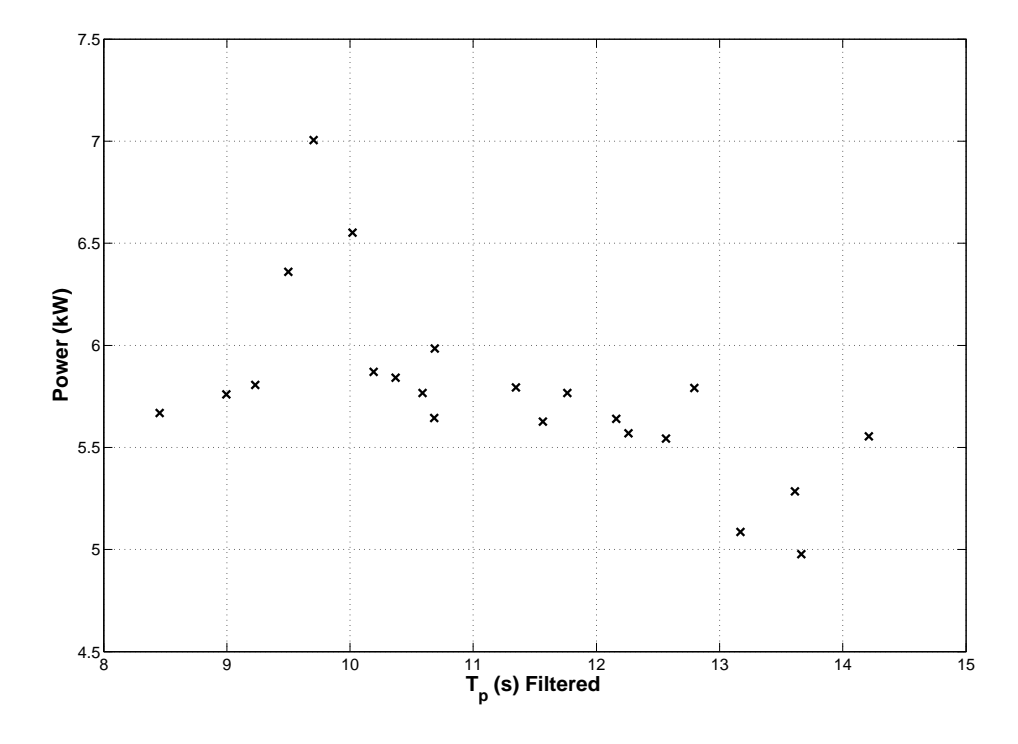


Figure 14: Maximum power generated  $(P_{gen})$  vs peak wave period for the hydraulic PTO

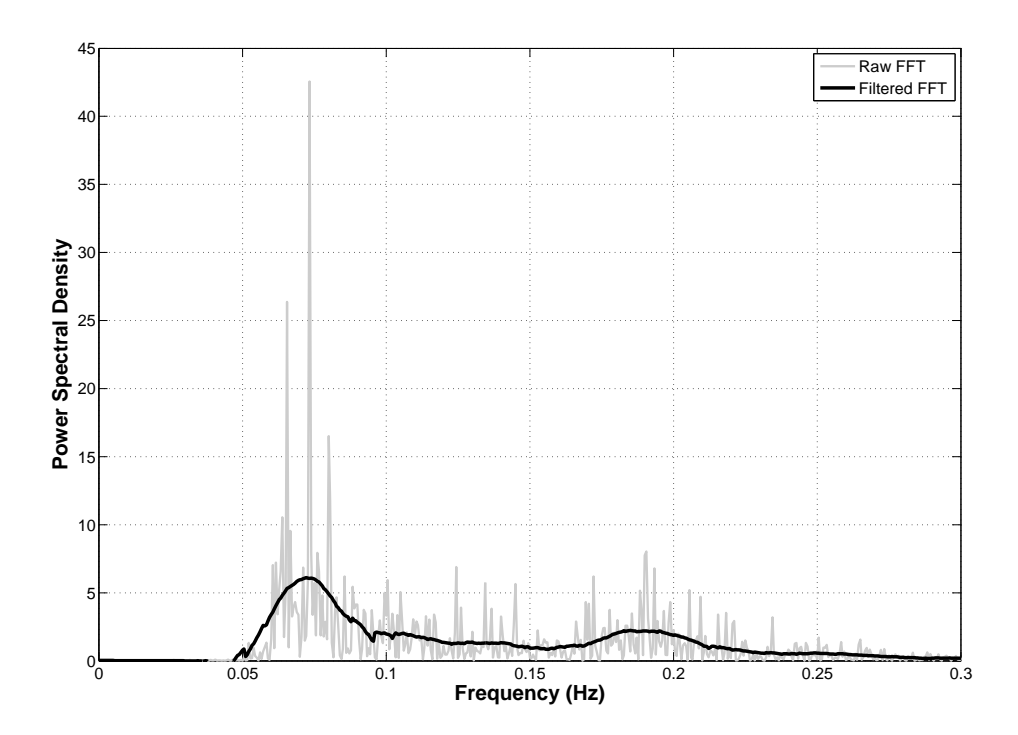


Figure 15: Frequency spectrum of one EMEC file with two distinct peaks

indicates that  $P_{gen}$  displays a minor drop with  $T_p$ , as previously demonstrated 229 in [3]. 230 Even with filtering, two distinct peaks may remain in the spectrum, like Figure 231 15, so the PTO may best be tuned to a frequency between these two peaks, 232 instead of the peak frequency, so it can benefit from the high energy at both 233 these frequencies. These types of spectrum are mainly responsible for the outliers 234 in Figures 10 and 11 and are the reason for the poorer correlation. The energy 235 period is less affected by these types of spectrum and therefore produces a better 236 correlation. It should be noted that sea states may exist in which little energy is 237 concentrated at  $T_p$  [19], in which case an iterative learning scheme aiming to 238 maximise measured power output by varying PTO and generator parameters would likely perform better. 240

#### 8. Real Time PTO tuning

Results suggest that a PTO can be tuned to maximise power generation by using  $T_e$  over a 30 minute time period. It is therefore beneficial to investigate the most suitable time period to use for tuning the PTO. Four EMEC files, that were not

used previously to determine the tuning trends, are chosen to investigate real time PTO tuning. Their parameters are presented in Table 4 and their filtered spectra are shown in Figure 16.

Wave Parameter	Sea States					
wave i arameter	1	2	3	4		
Date & Time	10/04 03:30	21/04 20:30	05/04 13:30	12/04 13:30		
$H_s$ (m)	1.24	1.98	3.10	4.34		
(Filtered) $T_p$ (s)	11.92	10.34	11.61	12.95		
$T_e$ (s)	10.18	9.72	8.83	10.45		

Table 4: Parameters of the four EMEC files chosen for the real time PTO tuning

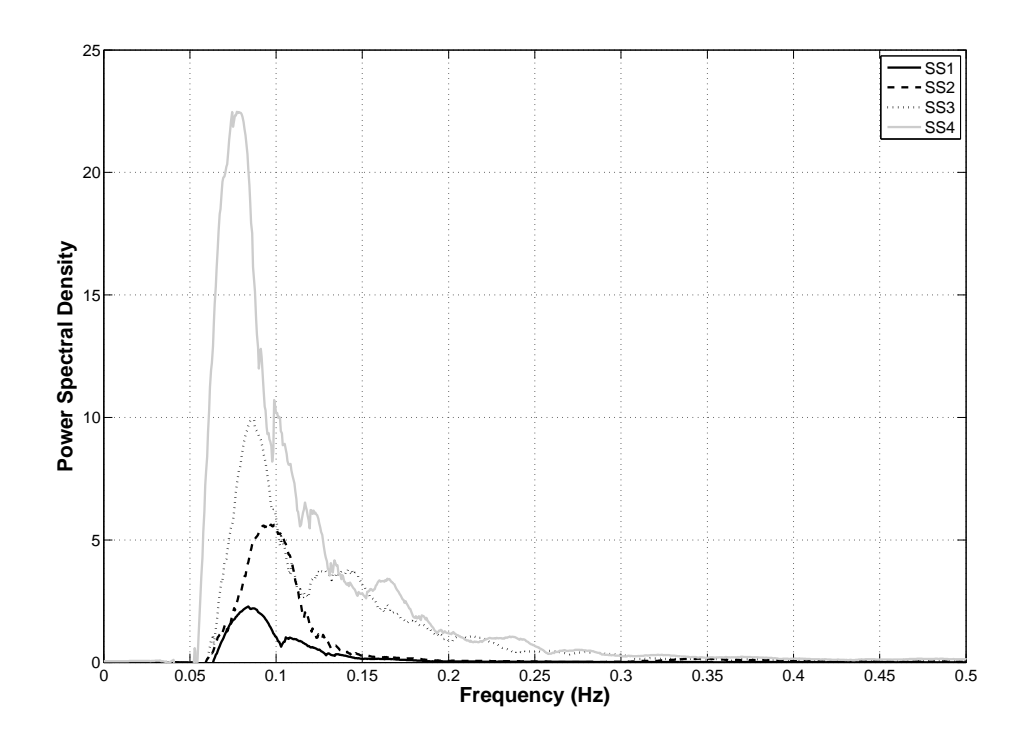


Figure 16: Filtered spectra of the four EMEC files chosen for the real time PTO tuning

Previous work into real time PTO tuning has shown an approximate doubling in power capture with a linear PTO by using an estimated wave frequency, calculated on a 20 s moving average, rather than the constant energy frequency of the spectrum [7]. The estimated wave frequency is calculated using a windowed FFT of the wave displacement. Furthermore, it has been shown that active tuning methods generally outperform passive methods with a linear PTO. Passive methods assume the PTO settings to be fixed whereas the active methods

assume that PTO settings can be constantly varying. In [8], an active tuning 255 technique is used with a 200 s window sliding FFT of the wave displacement. 256 Most recently, work has been presented which illustrates the advantages of 257 estimating the suitable wave frequency information by using signal processing 258 and filtering of the wave displacement signal [20]. It estimates the wave frequency information without future knowledge of the wave profile using the 260 zero-upcrossing method to update the linear PTO settings every 2-3s. The 261 zero-upcrossing method measures each point at which the wave profile crosses 262 the zero line upward. That point is taken as the start of an individual wave and 263 the next zero-upcrossing point is taken as the end of that wave. The time period 264 between the two adjacent zero-upcrossing points is defined as the wave period for 265 that individual wave and the vertical distance between the highest and lowest 266 points between the adjacent zero-upcrossing points is defined as the wave height. 267 In all these examples it is assumed that the PTO is linear and the desired 268 settings are achieved instantly. This work investigates methods to calculate wave 269 frequency information which is then used as the input to an open loop controller 270 for the tuning of the hydraulic PTO. Due to the good linear relationship, the 271 PTO damping  $(\alpha)$  is adjusted according to wave energy period  $T_e$  (see Figure 12). 272 A base-line passive method uses the PTO damping for the mean site energy 273 frequency  $(T_e=9.20\,\mathrm{s})$ . The mean site energy frequency is calculated from the 274 two months of data which have been collected. Four active methods are 275 investigated which assume that future prediction of wave displacement at the 276 WEC is not possible, so the PTO is tuned to the energy frequency calculated from a time period (window length) of preceding wave displacement data which 278 is updated every 20 s.

Strategy	Notation	Window Length
Passive	P	Site Average
	A1	30 mins
Active	A2	$10\mathrm{mins}$
Active	A3	$3\mathrm{mins}$
	A4	$30\mathrm{s}$

Table 5: Parameters of the five tuning strategies for the hydraulic PTO

The use of a doubly-fed induction generator (DFIG) is assumed (as is commonly

used in wind turbines) because they offer variable speed generation in an efficient 281 manner by using a frequency converter [21]. DFIGs have an operational range of 282 approximately  $\pm 30\%$  around the synchronous speed of 1500rpm, so it is assumed 283 that if the hydraulic motor speed is outside of this range no power can be 284 transmitted  $(P_{trans})$  to the grid and the generated power is wasted. A generator 285 efficiency of 100% is assumed. To maximise transmitted power, it is necessary to 286 maintain the hydraulic motor speed within the generator speed limits at all times 287 irrespective of wave conditions. The motor speed is controlled by adjusting its 288 displacement  $(x_m)$  using a proportional-integral (PI) controller acting on the 289 error in motor speed  $\omega_m$  from the synchronous value  $\omega_m$  with  $0.1 < x_m < 1.0$ . 290 Empirically tuned proportional and integral gains of 0.05 and 0.01 were used. 291 Changes to motor displacement  $(x_m)$  will be subject to the dynamics of the 292 swash plate positioning system of the hydraulic piston motor. It is assumed that 293 these dynamics can be modelled as a first order transfer function (R(s)) with a 294 time constant,  $\tau = 0.1 \,\mathrm{s}$ , such that 295

$$R(s) = \frac{1}{1 + 0.1s} \tag{26}$$

To ensure  $P_{cap}$  remains at its maximum,  $\alpha_{opt}(T_e)$  must be maintained whilst controlling the motor speed. To maintain  $\alpha_{opt}$  it is necessary to continually adjust the piston area or generator load at the same rate as  $x_m$ . Adjusting the generator load is the only feasible option so it must be varied alongside  $x_m$  to maintain  $\alpha_{opt}$  according to [3]

$$C_g = \alpha_{opt}(T_e) \left(\frac{x_m D_m}{A_p}\right)^2 \tag{27}$$

Therefore, in the simulation model the signal to alter the generator load is passed through the same transfer function (R(s)) or, in practice, an estimate of the real transfer function) to ensure both signals are in phase. The block diagram of this control strategy is shown in Figure 17.

In general, the results show that there is only a marginal gain, if any, from using active tuning methods (Tables 6 to 10). The captured power  $(P_{cap})$  is very similar for all the methods but there are slight variances in the generated  $(P_{qen})$ 

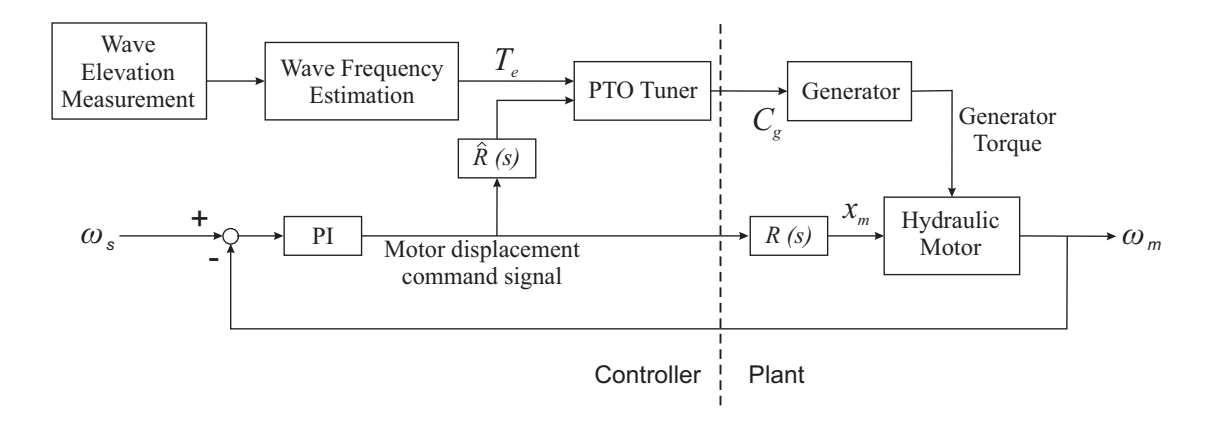


Figure 17: PTO Tuning and Motor Control Block Diagram

Strategy	Power (kW)			Efficiency (%)		
Strategy	$P_{cap}$	$P_{gen}$	$P_{trans}$	$\eta_{pto}$	$\eta_{trans}$	$\eta_{tot}$
P	1.13	0.18	0.18	16.2	98.7	16.0
A1	1.11	0.17	0.17	15.6	98.4	15.4
A2	1.12	0.18	0.17	15.7	98.6	15.5
A3	1.10	0.16	0.16	14.6	98.6	14.4
A4	1.10	0.16	0.16	14.6	98.5	14.4

Table 6: Results for SS1 comparing the different tuning methods

Strategy	Power (kW)			Efficiency (%)		
Dirategy	$P_{cap}$	$P_{gen}$	$P_{trans}$	$\eta_{pto}$	$\eta_{trans}$	$\eta_{tot}$
Р	6.21	3.41	3.40	54.8	99.7	54.7
A1	6.17	3.42	3.42	55.4	100	55.4
A2	6.16	3.42	3.42	55.4	100	55.4
A3	6.15	3.41	3.41	55.5	100	55.5
A4	6.16	3.41	3.38	55.3	99.2	55.3

Table 7: Results for SS2 comparing the different tuning methods

Strategy	Power (kW)			Efficiency (%)		
Strategy	$P_{cap}$	$P_{gen}$	$P_{trans}$	$\eta_{pto}$	$\eta_{trans}$	$\eta_{tot}$
Р	15.7	9.38	6.75	59.6	72.0	42.9
A1	15.8	9.26	6.48	58.6	70.0	41.0
A2	15.8	9.26	6.43	58.6	69.4	40.7
A3	15.8	9.32	6.67	59.0	71.5	42.2
A4	15.7	9.27	6.64	58.9	71.6	42.2

Table 8: Results for SS3 comparing the different tuning methods

Strategy	Power (kW)			Efficiency (%)		
Strategy	$P_{cap}$	$P_{gen}$	$P_{trans}$	$\eta_{pto}$	$\eta_{trans}$	$\eta_{tot}$
P	28.2	16.5	4.81	58.5	29.1	17.0
A1	28.3	17.4	6.43	61.4	37.0	22.7
A2	28.3	17.4	6.51	61.6	37.5	23.1
A3	28.3	17.3	6.27	61.2	36.2	22.2
A4	28.2	17.1	5.89	60.5	34.5	20.8

Table 9: Results for SS4 comparing the different tuning methods

Strategy		Sea S	States		Augraga
Strategy	1	2	3	4	Average
P			6.75	4.82	3.79
A1	0.17	3.42	6.48	6.43	4.12
A2	0.17	3.42	6.43	6.51	4.13
A3	0.16	3.41	6.67	6.27	4.13
A4	0.16	3.38	6.64	5.89	4.02

Table 10: The transmitted power in kW for each sea state using the active and passive tuning methods

and transmitted power  $(P_{trans})$ . The biggest gain is for the highest energy sea 308 state (SS4) where the active methods out perform the passive method by at least 309 20% (in terms of  $P_{trans}$ ). This is because  $T_e$  for SS4 has the biggest difference 310 from the site average value. 311 Figure 18 shows how the estimated energy period  $(T_e)$  and PTO damping  $(\alpha)$ 312 vary with time for the different control strategies. For A4 there are large 313 fluctuations in  $T_e$  between consecutive discrete values but these variations reduce 314 as the window length of the strategies increases. For SS4 the largest  $P_{trans}$  is for 315 method A2. For shorter window lengths, like A4, there can be large transient 316 waves which have a major affect on the estimated  $T_e$ . A2 gives a good balance 317 between tracking changes in  $T_e$  whilst not being biased by large individual waves. 318 The advantage of using a shorter window length is the reduction in the capacity 319 required to store preceding data but with the passive method there is no 320 requirement for data storage or online calculations. The results for these sea 321 states show only a minor reduction in transmitted power with the passive 322 method, but this would be exacerbated if the energy period differs significantly 323 from the average site value. 324 By way of illustration, Figure 19 shows a comparison of motor displacement

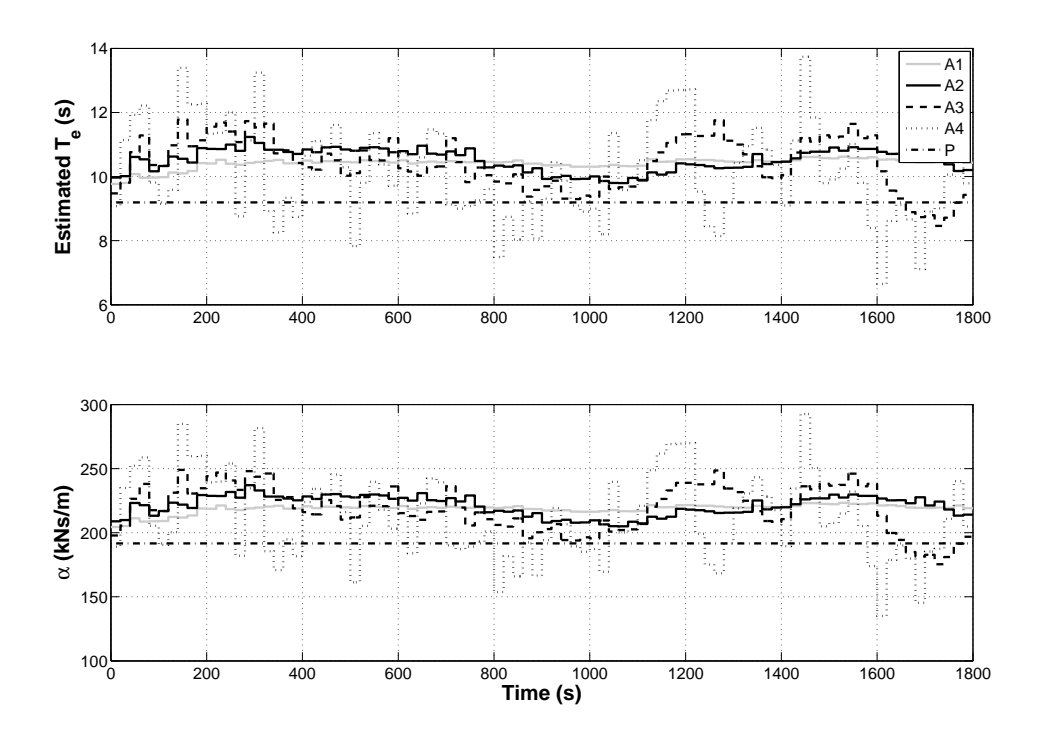


Figure 18: Estimated  $T_e$  and corresponding  $\alpha$  for the control strategies for SS4

fraction and motor speed for control strategies P and A4 for SS3. This shows how the motor displacement is varied in order to attempt to maintain the synchronous speed of the generator. Figure 20 shows the corresponding transmitted power for the different control strategies. It is clearly seen that transmitted power drops to zero when the synchronous speed limit of  $\pm 30\%$  is violated.

#### 9. PTO Tuning To Future Wave Data

Results show that active tuning of the PTO using preceding wave displacement 332 data does not provide a meaningful gain in  $P_{trans}$  compared to passive tuning to 333 a mean sea state. If the incident wave displacement could be predicted then 334 power increases could potentially be achieved. Previous work has shown this to be true for a linear PTO [8]. Here we investigate if this is also true for a realistic 336 hydraulic PTO model. 337 The tuning method predicts  $T_e$  from a future window length of 20 s and it uses 338 the previously identified trend to modify  $\alpha$  accordingly. The results, presented in 339 Table 11, indicate that there is only a small gain from using a future wave 340 prediction method when compared to the passive tuning method. The future 341

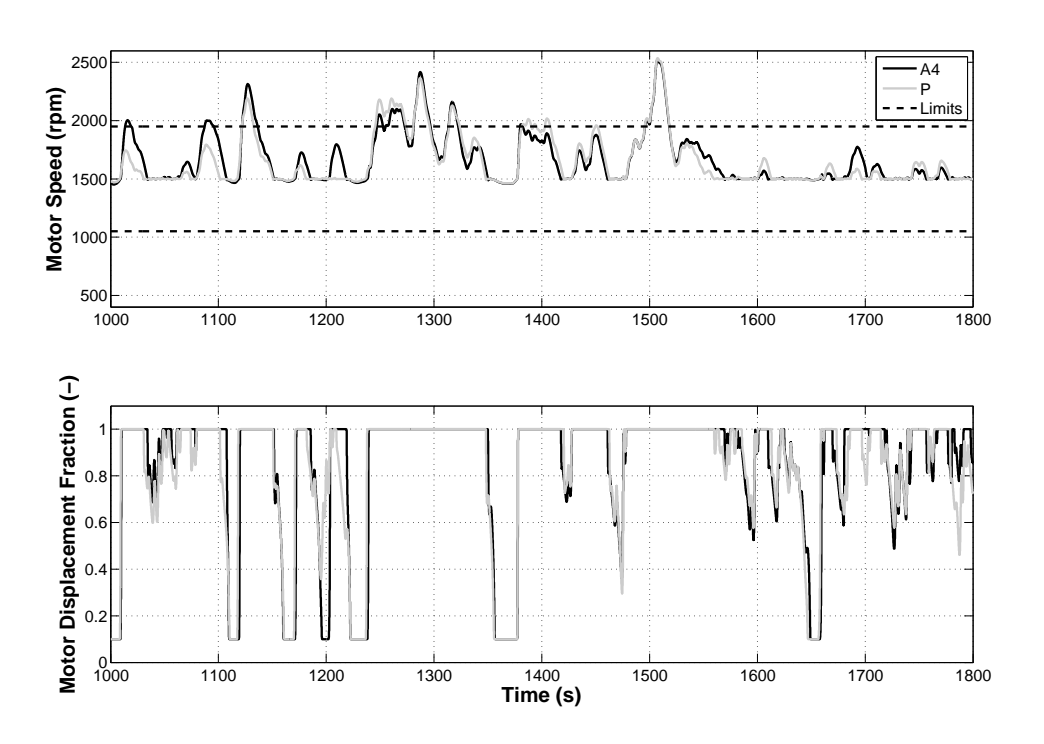


Figure 19: Comparison of motor displacement fraction and motor speed for control strategies P and A4 for  ${\rm SS3}$ 

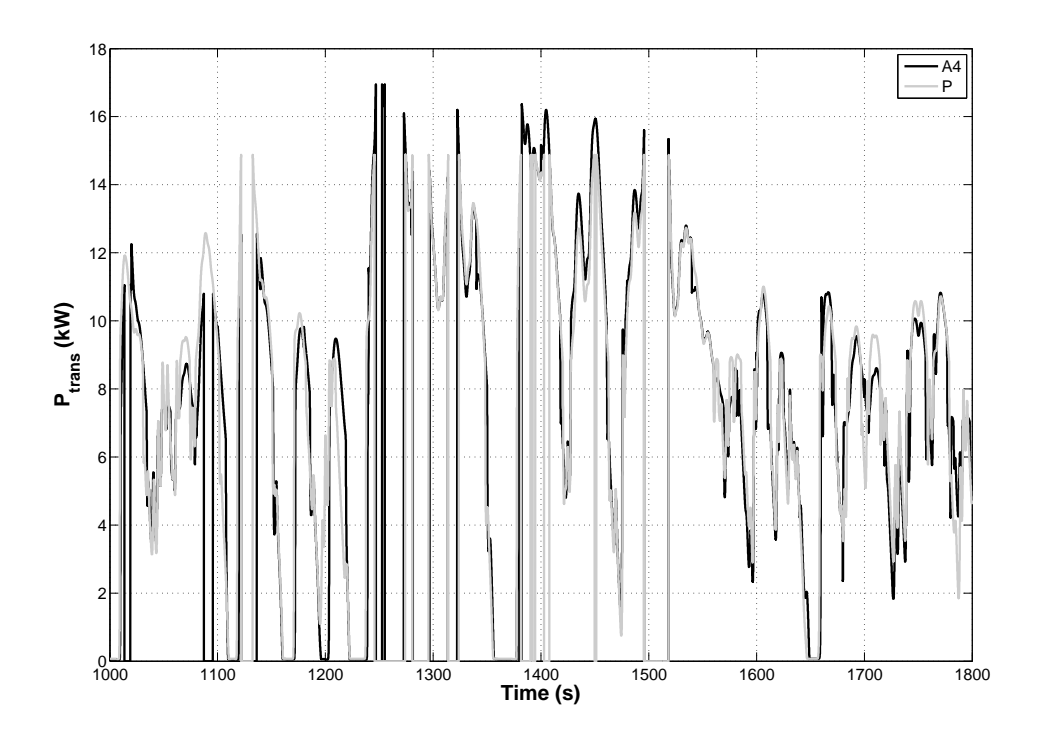


Figure 20: Comparison of transmitted power for control strategies P and A4 for SS3

prediction method only gives a higher transmitted power for SS4 compared to the passive method, but broadly speaking there is minimal change.

Strategy	Power (kW)	Sea States			
Durategy	Tower (KW)	1	2	3	4
	$P_{cap}$	0.97	6.19	15.7	28.4
Future	$P_{gen}$	0.11	3.38	8.99	17.1
	$P_{trans}$	0.10	3.37	5.79	5.41
	$P_{cap}$	1.13	6.21	15.7	28.2
Passive	$P_{gen}$	0.18	3.41	9.38	16.53
	$P_{trans}$	0.18	3.40	6.75	4.82

Table 11: The power for each sea state for the future and passive tuning methods

Therefore, this indicates that there is no gain from using algorithms or nearby measurement buoys to predict the future wave behaviour. Overall, the best tuning method is an active method which determines only a fundamental change in the energy frequency of the waves and therefore gradually changes the PTO damping to tune the device correctly. It is important to note that the presented  $P_{trans}$  values are still subject to the inefficiencies of the generator.

#### 10. Conclusions

```
Wave data for two months in 2011, recorded at the European Marine Energy
351
   Centre, was used to derive input data to evaluate tuning strategies for a realistic
352
   model of a hydraulic power take-off for a wave energy converter. The model was
353
   then used to determine the relationship between the peak wave and energy
354
   period and the optimum PTO damping for a number of sea states with varying
355
   parameters. An open loop active tuning method was investigated, in which past
356
   wave displacement data was used to adjust the PTO damping according to the
357
   wave energy frequency. Different window lengths were analysed for the active
358
   methods and compared to a passive method in which the PTO is fixed and tuned
359
   to the site average frequency. The investigation shows that the tuning of a
360
   hydraulic PTO to an estimated wave frequency is a difficult task. Even if the
361
   wave frequency can be estimated accurately and the PTO damping adjusted
362
   immediately, the PTO force will not change instantly due to the dynamics of the
363
   hydraulic PTO. The most effective active method analyses a sufficiently long
364
   preceding period of data to determine any change in significant wave frequency
365
   but not react to an individual wave. Power generation is expected to improve
366
   using active tuning as the energy frequency of the waves deviates further from
367
   the average site value. Preview knowledge of the future waves was shown to
368
   provide no meaningful improvement in energy capture for a point absorber WEC
369
   with a realistic PTO, though it would likely be of value for a wave-by-wave
370
   strategy such as latching control.
371
   Finally, the results have illustrated that there is a large power loss in the PTO.
372
   This is due to significant power loss in the components of the PTO (especially
   the hydraulic motor). For example, in low energy seas the small motor
374
   displacement required to maintain the synchronous speed means that the motor
375
   efficiency is always very low, so the mechanical power that is captured by the
376
   PTO can not be converted efficiently. Also, in high energy seas, there is a
377
   significant drop between the generated power and the transmitted power because
378
   the motor displacement is not large enough to maintain the synchronous speed.
379
   Therefore, even though the PTO efficiency may be adequate, a significant
```

portion of the generated power is lost. Significantly, power gains observed in similar work using simplified linear PTO models and/or simplified sea states are not seen here, demonstrating that over-simplification of the PTO during the simulation phase of WEC development could lead to incorrect design decisions and subsequent additional delay and cost.

#### 386 References

- [1] A.R. Plummer and M. Schlotter. Investigating the Performance of a

  Hydraulic Power Take-Off. In *Proceedings of the 8th European Wave and*Tidal Energy Conference (EWTEC), Uppsala, Sweden, 2009.
- [2] CJ Cargo, AR Plummer, AJ Hillis, and M Schlotter. Determination of optimal parameters for a hydraulic power take-off unit of a wave energy converter in regular waves. Proceedings of the Institution of Mechanical Engineers, Part A: Journal of Power and Energy, 226(1):98–111, 2012.
- [3] CJ Cargo, AJ Hillis, and AR Plummer. Optimisation and control of a hydraulic power take-off unit for a wave energy converter in irregular waves. Proceedings of the Institution of Mechanical Engineers, Part A: Journal of Power and Energy, 228(4):462–479, 2014.
- [4] A.F.O. Falcão. Modelling and control of oscillating-body wave energy
   converters with hydraulic power take-off and gas accumulator. Ocean
   Engineering, 34(14-15):2021–2032, 2007.
- [5] A.F.O. Falcão. Phase control through load control of oscillating-body wave
   energy converters with hydraulic PTO system. Ocean Engineering,
   35(3-4):358-366, 2008.
- [6] A. Babarit, G. Duclos, and A.H. Clément. Comparison of latching control strategies for a heaving wave energy device in random sea. *Applied Ocean*Research, 26(5):227–238, 2005.
- [7] H. Yavuz, A. McCabe, G. Aggidis, and M.B. Widden. Calculation of the performance of resonant wave energy converters in real seas. *Proceedings of*

- the Institution of Mechanical Engineers, Part M: Journal of Engineering for the Maritime Environment, 220(3):117–128, 2006.
- [8] H. Yavuz, T.J. Stallard, A.P. McCabe, and G. Aggidis. Time series
  analysis-based adaptive tuning techniques for a heaving wave energy
  converter in irregular seas. *Proceedings of the Institution of Mechanical*Engineers, Part A: Journal of Power and Energy, 221(1):77–90, 2007.
- [9] M. Folley and T. Whittaker. The control of wave energy converters using active bipolar damping. Proceedings of the Institution of Mechanical
  Engineers, Part M: Journal of Engineering for the Maritime Environment,
  223(4):479–487, 2009.
- [10] A. Babarit, M. Guglielmi, and A.H. Clément. Declutching control of a wave energy converter. *Ocean Engineering*, 36(12):1015–1024, 2009.
- [11] J. Falnes. Ocean Waves and Oscillating Systems: Linear Interactions
   including Wave-Energy Extraction. Cambridge University Press, Cambridge,
   UK, 2002.
- [12] A. Hulme. The Wave forces acting on a floating hemisphere undergoing
   forced periodic oscillations. The Journal of Fluid Mechanics, 121:443–463,
   1982.
- [13] S. Barstow, G. Mørk, D. Mollison, and J. Cruz. The Wave Energy Resource.
   In J. Cruz, editor, Ocean Wave Energy: Current Status and Future
   Perspectives, chapter 4, pages 93–132. Springer, 2008.
- 430 [14] W.E. Wilson. Performance criteria for positive displacement pumps and 431 fluid motors. *Trans. Am. Soc. Mech. Eng*, 71(2):115–120, 1949.
- [15] Edward Pitt. Assessment of Wave Energy Resource. Technical report,
   European Marine Energy Centre, 2009.
- [16] A. Savitzky and M.J.E. Golay. Smoothing and Differentiation of Data by
   Simplified Least Squares Procedures. Analytical Chemistry,
   36(8):1627–1639, 1964.

- [17] M.J. Ketabdari and A. Ranginkaman. Simulation of Random Irregular Sea
   Waves for Numerical and Physical Models Using Digital Filters. Transaction
   B: Mechanical Engineering, 16(3):240–247, 2009.
- 440 [18] AJ Hillis. Active motion control of fixed offshore platforms using an
  441 extended state observer. Proceedings of the Institution of Mechanical
  442 Engineers, Part I: Journal of Systems and Control Engineering,
  443 224(1):53–63, 2010.
- [19] A.D. de Andrés, R. Guanche, J. Weber, and R. Costello. Finding gaps on
   power production assessment on wecs: Wave definition analysis. *Renewable* Energy, 83:171–187, 2015.
- [20] H. Yavuz, S. Mistikoglu, and T. Stallard. Processing irregular wave
   measurements to enhance point absorber power capture performance. Ocean
   Engineering, 38(4):684–698, 2011.
- [21] A. Petersson. Analysis, Modeling and Control of Doubly-Fed Induction
   Generators for Wind Turbines. PhD thesis, Chalmers University of
   Technology, 2005.

# Nomenclature

## 454 Nomenclature

$A(\omega)$	frequency dependent added mass	[kg]
$A_p$	piston area	$[m^2]$
r	buoy radius	[m]
$B(\omega)$	frequency dependent radiation damping coefficient	[Ns/m]
$C_f$	motor coulomb friction coefficient	[-]
$C_g$	generator damping coefficient	[Nm/(rad/s)]
$C_v$	motor viscous friction coefficient	[-]
$D_m$	motor capacity	[cc/rev]
$f_c$	coulomb friction	[N]
$f_e$	wave excitation force	[N]
$f_{fr}$	cylinder friction	[N]
$f_h$	wave force	[N]
$f_{hs}$	wave hydrostatic force	[N]
$f_v$	viscous friction coefficient	[Ns/m]
$f_r$	wave radiation force	[N]
$F_e(s)$	Laplace transform of wave excitation force	[N]
g	gravitational acceleration	$[\mathrm{ms}^{-2}]$
H	wave height	[m]
$H_s$	significant wave height	[m]
J	generator inertia	$[\mathrm{kgm}^2]$
$K_v$	valve coefficient	$[\mathrm{m}^3/\mathrm{s}\mathrm{bar}]$
k	wave number	$[m^{-1}]$
l	half height of buoy	[m]
m	mass of buoy	[kg]
n	number of wave components	[-]
$p_i$	piston chamber pressure $(i = 1,2)$	[bar]
$p_A$	accumulator 'A' pressure	[bar]
$p_B$	accumulator 'B' pressure	[bar]
$P_{cap}$	captured power	[kW]
$P_{gen}$	generated power	[kW]

D	transmitted power	[kW]
$P_{trans}$	-	
$P_{wave}$	wave power	[kW]
$q_m$	flow rate to the motor	$[m^{3}/s]$
$S_n$	spectral density	$[\mathrm{m}^2\mathrm{s}]$
t	time	[s]
$T_m$	motor torque	[Nm]
$T_p$	peak period	[s]
x	buoy displacement	[m]
$x_m$	fraction of motor displacement	[-]
$\alpha$	PTO damping	[Ns/m]
$\alpha_{opt}$	optimum PTO damping	[Ns/m]
$\Delta t$	wave cycle time	[s]
$\Delta\omega$	wave frequency band	[rad/s]
$\epsilon$	Havelock's coefficient	[-]
$\eta_{pto}$	PTO efficiency	[%]
$\Gamma(\omega)$	wave excitation force coefficient	[N/m]
$\mu$	oil dynamic viscosity	$[\mathrm{Ns/m^2}]$
ho	water density	$[kg/m^3]$
$\Phi$	PTO force	[N]
$\omega$	wave frequency	[rad/s]
$\omega_m$	angular motor velocity	[rad/s]
$\omega_s$	generator synchronous velocity	[rad/s]
$\varphi$	wave phase component	[s]